Normal fluid stresses are prevalent in rotary Ventricular Assist Devices: a Computational Fluid Dynamics analysis

Short title: Normal fluid stresses in rotary Ventricular Assist Devices

Dominica P.Y. Khoo[1], Andrew N. Cookson[1], Harinderjit S. Gill[1], and Katharine H. Fraser*[1]

[1]Department of Mechanical Engineering, University of Bath, Bath, BA2 7AY, United Kingdom

*Corresponding author: Katharine H. Fraser

Department of Mechanical Engineering, University of Bath, Bath, BA2 7AY, United Kingdom

Email: k.h.fraser@bath.ac.uk.

Phone: 01225 384446

Word count: 5,814

Keywords: computational fluid dynamics, ventricular assist device, rotary blood pumps, shear stress, normal stress, elongational flow, blood damage

Abstract

Despite the evolution of Ventricular Assist Devices (VADs), VAD patients still suffer from complications due to the damage to blood by fluid dynamic stress. Since rotary VADs are assumed to exert mainly shear stress, studies of blood damage are based on shear flow experiments. However, measurements and simulations of cell and protein deformation show normal and shear stresses deform, and potentially damage, cells and proteins differently. The aim was to use computational fluid dynamics (CFD) to assess the prevalence of normal stress, in comparison with shear stress, in rotary VADs. Our calculations showed normal stresses do occur in rotary VADs: the fluid volumes experiencing normal stress above 10 Pa were 0.011 ml (0.092%) and 0.027 ml (0.39%) for the HeartWare HVAD and HeartMate II, and normal stresses over 100 Pa were present. However, the shear stress volumes were up to two orders of magnitude larger than the normal stress volumes. Considering thresholds for red blood cell and von Willebrand factor deformation by normal and shear stresses, the fluid volumes causing deformation by normal stress were between 2.5 and 5 times the size of those causing deformation by shear stress. The exposure times to the individual normal stress deformation regions were around 1 ms. The results clearly show, for the first time, that while blood within rotary VADs experiences more shear stress at much higher magnitudes as compared with normal stress, there is sufficient normal stress exposure present to cause deformation of, and potentially damage to, the blood components. This study is the first to quantify the fluid stress components in real blood contacting devices.

1 Introduction

Across the world an estimated 26 million people suffer from heart failure [1]. While for the majority of patients the condition is controlled using medical therapy, and in some cases a pacemaker or implantable cardioverter defibrillator may help, those with end-stage heart failure ultimately require a new heart. Ventricular Assist Devices (VADs) were developed to support the circulation until a suitable donor heart could be found (bridge-to-transplant), however, their success has also led to their use in patients not qualifying for a transplant (destination therapy) and, with over 5400 implants annually in the USA alone [2], they are now considered the gold standard treatment by some surgeons [3, 4]. The ultimate goal is heart recovery [5], although the number of patients who recover varies widely between centres, from close to 0% to over 50% [6, 7].

While there are a variety of VAD designs available, including both positive displacement VADs, such as the Berlin Heart Excor and the HeartMate XVE, and rotary VADs, which are currently favoured due to their small size and and robust mechanisms. Despite rotary VADs becoming an established therapy, serious complications can still arise [8]. Indeed, around half of all adverse events may relate to blood trauma [9] and the non-physiological flow conditions experienced by the blood are one major cause of that trauma: viscous stresses well above 50 Pa [10, 11] and turbulent (Reynolds) stresses above 100 Pa [11] are common in VADs, whereas wall shear stress (WSS) in the normal circulation is mostly under 2 Pa, ranging up to 15 Pa in the smallest vessels [12]. The large fluid dynamic stresses cause damage to the blood components; haemolysis, bleeding and thrombus formation are all significant problems resulting in increased hospitalisation, lower life expectancy and increased cost[13].

Fluid dynamic stresses arise from gradients in the velocity field. In general, fluid dynamic stress can be described by a tensor with six unique components: three of these give the normal stress and three give the shear stress. Imagining a cuboid of fluid, the normal stresses act perpendicular to the faces, whereas the shear forces act parallel to the faces. Normal forces work to create elongational (sometimes also called extensional)

and compressional flow fields, while shear forces create shear flows. Both elongational and shear flows can elongate the blood components, but do so in different ways. In attempting to understand the relationship between fluid dynamic stress and blood damage, the vast majority of work to date has been based on the assumption that in rotary VADs the dominant components of fluid stress are the shear stress components. Since rotary pumps involve sliding surfaces in close proximity which create shearing, the origin of this assumption is clear, however its validity has yet to be confirmed.

Furthermore, experimental measurements of the effects of shear and normal stress on red blood cells (RBCs) strongly suggest that normal stresses deform cells more than shear stresses. Lee *et al* [14] measured the deformation of RBCs in both shear and elongational velocity fields using a Couette flow device and hyperbolic converging microchannel respectively. They found that cell deformation, quantified by the deformation index DI ($DI = (L + W)/(L - W)$ where L is the cell's length and W its width) increased with either normal or shear stress and in both cases the deformation plateaued. However, the DI at the plateau was slightly higher, 0.6, for normal stress, compared with 0.5 for shear stress. Moreover, the minimum stress required to achieve a DI of 0.5 was 13.4 Pa with shear stress but only 1.8 Pa with normal stress. Yaginuma *et al* [15] and Zhao *et al* [16] also measured the deformation index of RBCs in elongational flow using similar converging channels with similar results.

There are far fewer investigations of cell damage, as opposed to cell deformation, under elongational flow. That said, there have been two important and similar studies. Down *et al* [17] used CFD to analyze the flow fields for capillary haemolysis experiments by Keshaviah [18]. The original experiments measured haemolysis in capillaries with different flow rates and entrance geometries, characterised by constriction ratio and tapering. Keshaviah concluded haemolysis was related to the entrance geometry, rather than the capillary diameter. Down *et al* [17] extended the analysis of the work by calculating the velocity fields, including the shear and normal stress components. They found no threshold shear stress for haemolysis, but all experiments had a similar threshold value for extensional stress, and they conclude extensional stress is a more critical parameter. The

second study by Yen *et al* [19] also investigated haemolysis in capillary tubes with varying constrictions. Yen *et al* [19] found that the flow weighted average maximum extensional stress along streamlines correlated with haemolysis, regardless of the entrance geometry. In contrast the correlation between shear stress and haemolysis differed between sharp and tapered capillary entrances.

The difference between shear and elongational flow effects on protein deformation are even more pronounced than those for cell deformation. Sing *et al* [20] performed coarse-grained molecular dynamics calculations to investigate the behaviour of von Willebrand factor (vWf) multimers in flow. vWf is a long molecule, up to 1000 μm in length [21]. When fluid dynamic stresses are low, the long chain molecule exists as a coiled globule, and in the presence of fluid dynamic stress the globule unravels to reveal the long chain. The percentage extension is used to quantify vWf deformation: $L/L_0 \times 100$ where L is the current length of the molecule and L_0 is the original length [20, 22]. Sing *et al* [20] found that a shear rate of 10^4 s^{-1} caused a 27 % extension of the vWf molecule but that an elongational rate of just 30 s^{-1} was enough to cause the same extension.

Numerical models for blood damage are generally based on the Scalar Shear Stress (SSS), a scalar invariant calculated from the tensor components in analogy with the von Mises stress for solids and first introduced by Bludszuweit [23]. Relationships between damage to the blood components and the SSS are then used in predictions of blood damage from the whole device. These methods make an assumption about the relative contribution from the normal and shear stress components to the scalar and hence to the blood damage. An alternative method, proposed by Arora et al [24], uses a fluid droplet model to estimate deformation, and hence damage to the RBCs, and has been implemented in both Lagrangian [25] and Eulerian [26] forms. The model overcomes the deficiency of using a scalar invariant to represent the stress tensor but as it uses a liquid droplet in place of a blood cell it still does not accurately estimate the differing contributions from shear and normal stress components.

Based on the available experimental data, numerical models for blood damage should account for the differing relative contributions of shear and normal stress components.

However, before proceeding to create such numerical models we wanted to establish their necessity; that is, do rotary VADs create normal stresses? Therefore, the aim of this work was to quantitatively assess the magnitude and extent of normal stresses present in commercially available rotary VADs and compare that with the magnitude and extent of the shear stresses. This assessment is vital in determining the importance of further experimental investigations of the influences of normal stress on the blood components, and of creating numerical blood damage models incorporating the influences of normal and shear stresses independently. To make this assessment we performed computational fluid dynamics (CFD) analyses on the two most commonly implanted VADs, the HVAD and the HeartMate II, and then used the velocity gradients to calculate the magnitudes of normal and shear stress components. The results reveal that while the magnitude of the normal stress is lower than the shear stress, there are substantial regions of normal stress in both VADs.

2 Methods

2.1 Geometry of the Flow Domain

Two commercially available rotary VADs were investigated: a centrifugal flow pump, the HVAD (Medtronic, formerly HeartWare, Miami Lakes, FL) and an axial flow pump, the HeartMate II (Abbott Laboratories, Abbott Park, IL, formerly Thoratec Corp, Pleasanton, CA).

The HVAD is now one of the most frequently used VADs and its small size allows implantation within the pericardium [27]. The main blood contacting components of the HVAD are an impeller with four wide blades, and a volute casing. The geometry and dimensions of these components (**Figure 1a**) were obtained from an explanted HVAD using a contact scanner (DS-10 Contact Scanner, Renishaw, Gloucestershire, UK). A computer aided model was then reconstructed from the scanned point cloud data in SolidWorks (SolidWorks 2015, Dassault Systems, Walton, MA, USA). In operation, the HVAD's impeller is suspended using hydrodynamic and magnetic levitation which maintains clearance between rotating and stationery parts. In this study, the impeller position was fixed so that

the top hydrodynamic bearing gap was 20 μm and the bottom, secondary flow, gap was 180 μm, which is appropriate for the operating conditions used [28]. However, the exact position of the rotating impeller still remains unknown due to the hydrodynamic thrust bearings. Since this position could have a large influence on the stresses, particularly the shear stress in the secondary and tertiary flow paths, the position of the impeller was varied to assess the impact on stress calculations.

The HeartMate II (HMII), has been implanted more times than any other VAD with over 20,000 implants to date [29]. The geometry of the HMII consists of a flow straightener, and an axial impeller and diffuser, each with three blades. The geometry (**Figure 1b**) was obtained from Fraser et al [10]. The impeller is held in place by blood washed cup-socket pivot bearings [30] which were not explicitly modelled. There was a fixed clearance gap of 100 μm between the housing and the blades.

To ensure fully developed flow at the entrance to the VADs, and to ensure the outlet boundary condition did not influence the flow within the VAD, the inlet and outlet tubes respectively were extended by at least 10 inlet radii when creating the computational fluid domain.

2.2 Mesh Construction

Unstructured hybrid meshes using tetrahedral, hexahedral and prism elements were constructed for each of the VADs using a combination of ANSYS Meshing (ANSYS Inc., Canonsburg, PA, USA) and TurboGrid (ANSYS Inc., Canonsburg, PA, USA). The sizes of the meshes were, HVAD: 8.5M and HMII: 2.52M elements. The design of the HMII makes hexahedra easier to implement, and most of the domain was meshed using this efficient element shape, hence the mesh size is smaller than that for the HVAD. Each mesh had a minimum of 6 elements across the gaps. Because regions of high stresses are of special interest, inflation layers were generated near the walls of both housing and rotor to resolve the near wall flow.

Discretisation errors were assessed using coarser and finer meshes. Refinement ratios of 2 (coarse mesh, 3.8M elements) and 0.5 (fine mesh, 18.1M elements) to yield three meshes

for the centrifugal VAD. The discretisation errors were assessed by examining pressure heads, velocity fields and fluid dynamic stresses volumes. The same analysis method was applied to the axial VAD using refinement ratios of 1.25 (coarse mesh, 1.3M elements) and 0.625 (fine mesh, 5.6M elements).

2.3 Computational Fluid Dynamics

The Unsteady Reynolds Averaged Navier-Stokes (URANS) equations were solved using a commercial, vertex-centered, finite volume solver ANSYS CFX (ANSYS Inc., Canonsburg, PA, USA). The largest Reynolds number at the inlet was 2530 which is above transition to turbulence (usually taken to occur around 2300 for pipe flow) and in the low turbulence flow regime. The k-ω shear stress transport model was used to model the turbulence. The operating points chosen for the calculations were based around a typical working point for LVADs: 5 l/min at 100 mmHg which required an impeller rotational speed of 3000 rpm. The inlet boundary condition was mass flow rate, fixed to give flow rates of 3, 5 or 7 l/min, with speed set at 3000 rpm. The rotational speed was varied from 2200 to 3400 rpm, while maintaining 5 l/min. The outlet boundary condition was constant, uniform pressure at 0 mmHg. Blood was treated as a Newtonian fluid with density of 1050 kg/m^3 and dynamic viscosity of 3.5 mPas.

Transient calculations were used and the rotation of the impeller was accounted for by using sliding meshes, also known as the transient rotor-stator approach. These transient calculations were initialised from steady-state calculations in which the motion of the impeller was incorporated using the multiple reference frame (MRF) approach. The time step for the transient calculations was adjusted with respect to the rotational speed to yield 2° rotation per step. These calculations were run using high resolution, and second order backward Euler, schemes in space and time respectively, for three full rotations. Following the first rotation the pressure head showed a smooth periodic behaviour. The averaged pressure head and velocity field were obtained from the third rotation.

2.4 Validation

For validation of the numerical model, the calculated pressure-flow plots were compared with published experimental data for steady flow in the HVAD and HMII [31]. To date there are no published experimental data on the velocity fields for either the HVAD and HMII, for the real scale. Therefore, a benchmark blood pump obtained from the US FDA [32] was modelled using a mesh created with the same principles as described in section 2.2 and with the flow calculated using the methods given in section 2.3. The operating condition was an angular velocity of 3500 rpm with flow rate of 6 l/min. The quantitative validation then compared velocity plots from specific regions of the blood pump with published Particle Image Velocimetry (PIV) results.

2.5 Post Processing

2.5.1 Coordinate Transformation of Stress

The viscous stresses of specific interest are shear stress and normal stress, which, based on the literature, are thought to differently deform and damage the blood cells and proteins. According to Lee *et al* [14] shear stress will first cause the cell to be rotated and then deformed, while normal stress will deform the cell without rotation. For a Newtonian fluid the viscous stresses are proportional to the strain rates and are described by a symmetric tensor, which varies depending on the reference frame $\tau_{ij} = 2\mu \mathbf{s}_{ij}$ (where $\mathbf{s}_{ij}$ is the deformation, or strain rate $\mathbf{s}_{ij} = \frac{1}{2}\left(\frac{\partial u_i}{\partial x_j} + \frac{\partial u_j}{\partial x_i}\right)$). However, the stress experienced by the blood should not depend on the reference frame. We defined a local coordinate system for every point in the flow domain which had x_1' aligned to the velocity vector at that point. The rotation from the original velocity vector $\mathbf{u} = (u_1, u_2, u_3)$ to the velocity vector $\mathbf{u}' = (|\mathbf{u}|, 0, 0)$ in the new coordinate system is unique. The rotation matrix $\mathbf{R}$ defining the rotation from $\mathbf{u}$ to $\mathbf{u}'$ was constructed for each point according to Rodrigues Rotation Equation [33]:

$$\mathbf{R} = \cos\theta \mathbf{I} + \sin\theta \mathbf{n}_\times + (1 - \cos\theta)\,\mathbf{n}\mathbf{n}^T \tag{1}$$

where θ is the angle between $\mathbf{u}$ and $\mathbf{u}'$, $\mathbf{I}$ is the identity matrix, $\mathbf{n}$ is the axis of rotation about which θ is defined, and $\mathbf{n}_\times$ is the cross product matrix for $\mathbf{n}$ (details in Appendix).

$\mathbf{R}$ was then used to rotate the strain rate tensor $\mathbf{s}_{ij}$ for that point into the local coordinate system $\mathbf{s'}_{ij}$:

$$\mathbf{s'} = \mathbf{RsR}^T \tag{2}$$

The normal stress was then found directly from the strain rate component $\mathbf{s'}_{11}$

$$\tau'_{11} = 2\mu s'_{11} \tag{3}$$

Then positive values of τ'_{11} correspond to a normal stress which tends to elongate the flow in the direction of the velocity, such as would be found at the constricting entrance to a nozzle, or needle, or potentially in leakage over a blade tip. Negative values of τ'_{11} correspond to compressive normal stress in the direction of the velocity, such as that at the diffusing exit of a nozzle. The shear stress was found from the strain rate components s'_{12} and s'_{13}:

$$\tau'_{12/13} = 2\mu \left(s'^2_{12} + s'^2_{13} \right)^{\frac{1}{2}} \tag{4}$$

$\tau'_{12/13}$ is the magnitude of the shear stress resulting from u'_1 gradients in the x'_2 and x'_3 directions.

2.5.2 Fluid Stress Threshold Volumes

To assess both the magnitude and extent of the normal stress τ'_{11}, relative to the shear stress $\tau'_{12/13}$, the flow domain was thresholded into regions with stress values greater than 10, 50 and 100 Pa. While blood damage processes are complicated functions of both stress magnitude and exposure time, these values were chosen as representative values for low, middle and high stress. Based on the published data: 10 Pa is thought to be relevant to the cleavage of vWf [34, 35, 36], which is the blood damage aspect of bleeding events; 100 Pa is thought to be relevant to haemolysis [37, 38, 39]; and 50 Pa is an intermediate threshold. The values are not intended to be exact, but are a way to quantitatively compare the stress fields in different VADs. The thresholded regions were displayed in CFX Post (ANSYS Inc., Canonsburg, PA, USA) to determine where the stresses occurred.

For quantitative comparison the volumes of the thresholded regions were calculated. Since the simulations were transient, the volumes were found every 20° of impeller rotation, and

these volumes were averaged for comparisons.

2.5.3 Cell Deformation and Protein Unravelling Threshold Volumes

Since the available data suggest cell deformation [14] and protein unravelling [20] occur at lower elongation stress, compared to shear stress, we assessed the volumes which could deform cells and unravel proteins. Regarding RBC deformation, Lee *at el* [14] measured cell deformation as a function of either shear or normal stress. We used this data to find stress values which would create a DI of 0.5 (**Figure 2a**). A DI of 0.5 is achieved with shear stress of 13.4 Pa, whereas the value with normal stress is much lower at 1.8 Pa. Regions of the VADs with $DI > 0.5$ were compared for shear and normal stress by thresholding at 13.4 Pa and 1.8 Pa respectively.

Thresholds for unravelling vWf come from work by Sing *at el* [20] who used a coarse-grained numerical model to investigate the hydrodynamic forces on vWf molecule. In their study a 27% extension of the vWf molecule was obtained with a shear rate of 10^4 s^{-1}, or an extensional rate two orders of magnitude lower at 200 s^{-1} (**Figure 2b**). These correspond to stresses of 35 Pa and 0.7 Pa respectively for the CFD calculations presented here.

2.5.4 Exposure times

Fluid stresses act in combination with exposure times to cause deformation of, and eventually damage to, the blood components. To estimate the exposure time of the blood components to both normal, and shear, stress, pathlines were calculated from the final timestep of the solution. The final timestep was chosen since the volumes of the high stress regions were not found to vary significantly with time. Pathlines were seeded in the regions of cell deformation and protein unravelling described above, and were tracked both forwards and backwards using a Runga-Kutta method with a tolerance of 1 % of the mesh element size. The length of time within the region was calculated for each pathline and the mean was then found. The total number of pathlines used was 2000. This value was chosen based on a convergence test using the RBC deformation regions in the HVAD. Reducing the number of pathlines to 500 resulted in a reduction in the normal

stress exposure time of almost 10 %, while increasing the number to 8000 resulted in an increase in that exposure time of around 5 %. There was almost no change in the shear stress exposure times over this range in number of pathlines. This increase in normal stress exposure time with the number of tracks suggests our analysis is more likely to under, rather than over, estimate the normal stress exposure time.

3 Results

3.1 Mesh Sensitivity

The mesh discretization error was assessed by comparing pressure head, velocity fields and stress volumes using the three meshes, with the operating condition 3000 rpm, 5 l/min and with the steady state (multiple reference frame) calculations. The pressure heads were 107.7 mmHg, 105.9 mmHg, and 105.2 mmHg with coarse, medium and fine meshes respectively, giving a percentage error of 0.6% between medium and fine meshes. For qualitative comparison the velocity fields are shown in **Figure 3a**. Differences between coarse and medium meshes can be seen, for example in the south pointing blade gap, but are more difficult to spot between medium and fine meshes. Due to their direct dependence on velocity gradients the fluid stress is more sensitive to discretization error than the velocity. The percentage difference between medium and fine meshes was 8.9% and 5.7% for the normal and shear stress volumes at 50 Pa respectively. The percentage difference between medium and fine meshes was 0.6% and 3% for the normal and shear RBC deformation volumes respectively. The medium mesh was used as it had an acceptable balance between computational resources and accuracy (**Figure 3b and 3c**).

3.2 Validation

The calculated pressure heads were in good agreement with experimental data from Noor *at el* [31] with an average percentage error of less than 5% (**Figure 4**). There are no published experimental data for the velocity field in the HVAD. Therefore, to validate the CFD method, here the flow field for the FDA Benchmark blood pump was solved and the calculated velocity fields were compared with the published PIV results [32]. There

is reasonable qualitative agreement in the velocity fields and an average 4.6% error as compared to the measurements (**Figure 5**).

3.3 Fluid Stress Threshold Volumes

In the HVAD the highest shear stress was found in the narrow axial hydrodynamic bearing gap clearance of 20 μm above the impeller (**Figure 6**). Shear stress in this region was in the range 100 Pa to 1000 Pa. Other regions with high shear stress were the gap under the impeller (shear stress up to ∼80 Pa), shear stress on the volute wall was in the range 0 to 60 Pa, and there were regions of high shear within the blade passages (up to ∼15 Pa). The bulk of the volute experienced shear stress in the range 2 to 6 Pa. Similarly the highest normal stresses (up to ∼100 Pa) were also found in the hydrodynamic bearing gap, specifically in the regions of the narrowest part of the gap where blood leaks over the edges of the hydrodynamic blades and tiny regions at the tips of the leading edges of the blades. Normal stress up to around 15 Pa were found in the inter blade passages where, due to a recirculation zone which narrows the passageway, the forward flow is forced to accelerate. There was also a stagnation point at the flow divider between outlet and re-entering volute where both high shear and high normal stresses occurred (up to 23 and 33 Pa respectively).

In the HMII the highest shear stresses were found in the blade tip gaps (up to ∼400 Pa), whereas the negative, low pressure side of the blade experienced the highest normal stress (up to ∼100 Pa) along the curvature of the blade. High velocity regions (between 5 to 8 m/s) at mid-section of the impeller and housing also experienced shear stress. In the diffuser section the highest normal stresses are between the hub and the blades (up to ∼50 Pa).

Blood in both VADs clearly experienced higher shear stress over a larger volume as compared to normal stress. In the HVAD the volume at 10 Pa was almost two orders of magnitude higher for shear stress compared to normal stress (0.74 cm^3 compared to 0.011 cm^3) while at 100 Pa the difference is three orders of magnitude (0.020 cm^3 compared to 0.000015 cm^3). In the HMII the differences between shear and normal stress volumes were similar, with the shear volume still always larger (0.86 cm^3 compared to 0.027 cm^3 at

10 Pa, and 0.10 cm^3 compared to 0.00077 cm^3 at 100 Pa). Both shear and normal stress volumes were larger in the HMII compared with the HVAD. The internal fluid volumes of the two VADs are similar: the HVAD is 12 cm^3 and the HMII is 7 cm^3.

3.4 Cell and Protein Deformation Threshold Volumes

Since the literature suggests lower normal stresses cause cell deformation and protein unravelling, compared with shear stress, the fluid volume was thresholded based on RBC and vWf deformation. For cell deformation the values used were 13.4 Pa for shear stress and 1.8 Pa for normal stress (**Figure 7**). In the HVAD the RBC deformation volume was larger for shear stress as compared with normal stress (0.61 cm^3 compared to 0.46 cm^3) whereas in the HMII the shear stress volume was smaller than the normal stress volume (0.46 cm^3 compared to 0.80 cm^3). The vWf deformation volume was much larger for normal stress as compared with shear stress: 5 times the size (0.99 cm^3 compared to 0.18 cm^3) for the HVAD and 2.5 times the size (0.75 cm^3 compared to 0.31 cm^3) for the HMII.

The variation in cell deformation volume over time, as the impeller rotates, was investigated by plotting the volumes every 20° interval (which is every 10 time steps or 1.1 ms). The cell deformation volume due to shear stress was constant over time. The shear stress occurred mostly in the gap clearances above and below the impeller which do not change with time. The cell deformation volume due to normal stress was a repetitive continuous wave because of the rotating impeller with peak volume of 0.47 cm^3 and minimum volume of 0.45 cm^3. The peak occurred at 60°, which corresponds to the blade passage pointing directly at the cutwater. Recurring regions of normal stress at this threshold occurred in the volute, at the wall of the impeller, and in between the blades along the slope.

3.5 Exposure Times

Using the pathline based approach, the mean exposure times of blood in the two VADs to levels of normal and shear stress sufficient to deform RBCs and vWf were found (Table 1). The duration of exposure to shear stress is clearly longer than that to normal stress, however, the exposure times for normal stress were not insignificant at around 1 to 2 ms

depending on the VAD and blood component of interest. It is also worth noting that while the shear stress exposure times were almost identical for both VADs, the normal stress exposure times in the HMII were double those in the HVAD. Considering only the shear stress in the VADs would make these two appear similar, in terms of damage performance, which could imply that potential differences in their safety, related to the normal stress, would be missed.

3.6 Influence of Operating Condition: Flow Rate and Impeller Speed

The difference in the cell deformation volume was investigated for varying operating conditions (**Figure 8**). As the rotational speed was increased, with constant flow rate of 5 L/min, the cell deformation volumes for both normal and shear stress increased with the normal RBC deformation volume reaching 0.50 cm^3 and shear volume reaching 0.63 cm^3 at a speed of 3400 rpm. The pathline analysis showed that the exposure times for the normal stress deformation volumes were roughly constant with changes in speed whereas the exposure times for the shear stress deformation volumes decreased by a factor of two between 2200 and 3400 rpm.

The deformation volumes also depended on the flow rate. Increasing flow rate from 3 to 7 l/min, with impeller speed constant at 3000 rpm caused a tiny increase in shear stress volume from 0.58 cm^3 to 0.64 cm^3. The influence of flow rate on elongational cell deformation volume was more significant: the increase from 3 l/min to 7 l/min caused the RBC deformation volume to increase from 0.39 cm^3 to 0.54 cm^3. In the case of flow variation the pathline analysis showed the opposite trends as compared to those for speed variation. The exposure times for the shear deformation volumes were constant with changes in flow, likely because the small increase in the size of the deformation volume was countered by the increasing average speed through the VAD with flow rate. However, the exposure times for normal stress deformation volumes increased by a factor of five between 3 and 7 l/min, showing the larger increase in the size of the deformation volume was the important effect in this case.

3.7 Influence of Axial Clearance Gap

The HVAD impeller is hydrodynamically suspended, so the clearance gaps vary with operating condition. The gap used in the study was 20 μm [28] but to assess the impact of any possible error, the gap was varied from 20 to 100 μm (with operating condition: 5 l/min at 3000 rpm). The cell deformation volume due to normal stress decreased slightly (from 0.46 cm^3 to 0.44 cm^3) as the axial gap clearance increased, whereas the cell deformation volume due to shear stress remained constant. This difference did not cause a change to the exposure times, and is not enough to influence the conclusions.

4 Discussion

Fluid stresses are well known to be a major cause of blood damage in rotary VADs [10]. As discussed in section 2.5.3, the different components of the stress deform and damage the blood components differently, with normal stress causing larger cell and protein deformations at smaller stress magnitudes as compared with shear stress [14, 15, 16, 20]. There have been many studies measuring the effects of shear stress on blood damage [40, 39, 41, 38, 37] but far fewer on the effects of normal stress [17, 19]. Before embarking on such studies we wanted to find out how significant the problem of normal stress in rotary VADs might be. Therefore, the aim of this study was to assess the prevalence of normal stress as compared with shear stress in the most commonly implanted rotary VADs. CFD calculations were performed for the HVAD, a centrifugal blood pump, and the HMII, an axial blood pump, and the normal and shear stresses were calculated.

The results of the calculations showed there are large regions experiencing high shear stress magnitudes in both VADs: the volume above 10 Pa was 0.74 cm^3 (6.2 %) and 0.86 cm^3 (12 %) for the HVAD and HMII respectively. A value of 10 Pa is above the level of the WSS in the vast majority of the normal healthy cardiovascular system [12]. The volumes with a shear stress above 50 Pa, which is well above the WSS in the whole normal circulation were 0.075 cm^3 (0.63 %) and 0.228 cm^3 (3.3 %) for the HVAD and HMII respectively. The volumes above 100 Pa, enough to cause haemolysis, were 0.020 cm^3 and 0.03 cm^3.

In contrast the volumes experiencing normal stress at the same threshold values were much smaller: above 10 Pa the volumes were 0.011 cm^3 (0.092 %) and 0.027 cm^3 (0.39 %) for the HVAD and HMII respectively. A 10 Pa normal stress is sufficient to cause maximal cell deformation [14] and protein unravelling [20]. The volumes with normal stress above 100 Pa were 0.000015 cm^3 (1.3×10^{-4} %) and 0.00077 cm^3 (0.011 %) for the HVAD and HMII. So, the shear stress magnitudes are clearly greater than normal stress magnitudes, and the volume of the fluid domain experiencing these high values is larger for shear stress than for normal stress. This is logical since the devices are rotating with small gaps that creating a shearing action. Available data for the effects of normal stress on haemolysis come from Down *et al* [17] and Yen *et al* [19]. The study by Yen *et al* [19] implies normal stress of at least 1000 Pa is required to cause 1% haemolysis. However, the exposure time is lower in both of these capillary entrance experiments [17, 19] as compared with the VADs, in which recirculation is also possible. The residence time in the very high normal stress regions ($>$ 1000 Pa) in these works can be estimated as 0.003 ms [17] and 0.06 ms [19], in contrast with average times of 0.87 to 2.1 ms in the cell deformation regions found here, and with average total times of 144 ms and 84 ms in the HVAD and HMII respectively [42]. There are no experimental studies which measured thresholds for haemolysis with normal stress exposure times around 1 ms.

Given that the available literature for cell and protein deformation [14, 20] shows that these deformations occur at lower normal stress magnitudes than shear stress magnitudes, the fluid volumes were thresholded according to deformation. When the RBC deformation threshold of DI=0.5 was applied, the cell deformation volumes were 1.5 to 2 times larger for normal stress as compared with shear stress. The exposure times were smaller for normal stress, between 0.87 and 2.1 ms, which is 7 to 17 % of the shear stress times. These normal stress exposure times can be compared with estimated exposure times from the work by Yaginuma *et al* [15]. Based on the data given in that work the exposure time for cells to reach DI=0.35 was 1.7 ms and therefore the exposure times calculated here are likely to be sufficient to cause cell deformation.

Differences in deformation volume were even more pronounced when considering vWf de-

formation: when the vWf extension threshold of 27% was applied, the vWf deformation volumes were 5 to 20 times larger for normal stress as compared with shear stress. Again the exposure times were smaller for normal stress, between 1.1 and 2.5 ms, which is 12 to 30 % of the shear stress exposure times. There are no studies of exposure time on vWf deformation to compare with.

To compare our simulations with those already published we calculated the Scalar Shear Stress [23], a scalar invariant quantifying the stress magnitude:

$$\tau_{SSS} = \left[\frac{1}{6}\left(\left(\tau_{11}-\tau_{22}\right)^2+\left(\tau_{22}-\tau_{33}\right)^2+\left(\tau_{33}-\tau_{11}\right)^2\right)+\tau_{12}+\tau_{23}+\tau_{31}\right]^{\frac{1}{2}} \tag{5}$$

Volumes of SSS were in good agreement. For the HMII the volume above 9 Pa was 1.6 ml, compared to 1.7 ml [11] and 2.1 ml [10] and at 50 Pa was 0.32 ml, compared to 0.3 ml [11] and 0.42 ml [10].

This investigation showed that normal stresses are present in rotary VADs. Furthermore, while the magnitudes and exposure times for the normal stresses are lower than the shear stresses, there is sufficient normal stress magnitude, for a long enough exposure time, to cause cell and protein deformation. This finding suggests that damage to the blood components caused by the normal stress components is an important consideration for the design of VADs and the development of blood damage models. The results of our investigation then justify further experimental studies into the effects of normal stress, and normal stress in combination with shear stress, on the blood components. The results of these future experiments would enable the proper incorporation of the effects of normal stress into numerical blood damage models.

4.1 Limitations

This investigation was designed to calculate normal stress experienced by blood in the direction of the flow, analogous to the type of normal stress experienced when blood enters a narrow constriction, such as at the entrance to a needle or through an arterial stenosis. From the literature this type of normal stress stretches RBCs, in the direction of the flow, and unravels vWf. The study was not designed to calculate normal stress in the

directions perpendicular to travel. This type of normal stress would be experienced by blood when the shape of the channel changed, such as if the shape of a channel changed from a vertical to a horizontal slot of the same cross sectional area. It seems possible that this type of normal stress would similarly deform RBCs, elongating them perpendicular to the direction of travel. However, there are no experimental results in the literature related to this scenario. Furthermore, blood damage effects, including RBC deformation and unravelling of vWf molecules, depend on changes in fluid stress with time, which occur due to the blood transiting regions with spatial shear stress gradients. These effects were not the subject of this study, but could be investigated in future, using particle based models (see for example [25, 43, 44]).

As explained in section 2.3 the unsteady Reynolds Averaged Navier-Stokes equations were solved with the SST k-ω model for turbulence. This was because, with a 5 l/min flow rate, Re at the straight tube inlet was 2530, which is above the critical threshold for transition to turbulence in a straight tube, usually taken to be 2300. However, turbulence models are designed for high Re turbulence, which could result in some errors in the mean flow field. These are likely to be small and would effect both shear and normal stresses similarly. The turbulent shear and normal stresses (components of the Reynolds stress) were not included in this investigation since the literature on the effects of turbulent stresses is inconclusive.

Blood is well known to be a multiphase, shear thinning fluid, however in this work it was treated as a single phase Newtonian fluid. The shear thinning viscosity has the potential to increase shear rates near the walls which would have a small effect on the shear stress calculation. Additionally, haematocrit in the gap regions between the impeller and housing has been shown to be lower compared with that in the bulk flow [45]. This causes reduced viscosity in these regions so would reduce the, predominantly, shear stresses found there.

Pathlines calculated from one simulation timestep were used to estimate the duration of exposure of blood to the various stress threshold levels. Since these are transient simulations a more correct approach would have been to calculate time dependent particle tracks, initiated from the inlet of the flow domain and tracked with the flow to the outlet.

However, only a small portion of the flow passes through the high stress regions, many of which are located in the secondary flow path, so in order to achieve a representative number of tracks which encountered these high stress regions a vast number more would need to have been seeded. We used 2000 pathlines, but with particle tracking, the number of particle tracks initiated from the inlet would have had to be much larger. The pathline approach is justified in this work since the maximum exposure time for normal stress is equivalent to 45^o rotation of the impeller which, with the exception of the region near the cut water, has only small changes in the velocity field. The pathline based approach is therefore likely to be most accurate for the normal stresses, but might overestimate the exposure to shear stresses which have longer exposure times over which the velocity field would change more. It is also important to note that the method only looked at exposure to individual high deformation regions. In reality the blood components would be exposed to multiple regions of high stress, so the total exposure times would be considerably longer.

5 Conclusion

Based on these calculations normal stresses do occur in rotary VADs. The fluid volume experiencing normal stress above 10 Pa was 0.011 cm^3 and 0.027 cm^3 for HVAD and HMII respectively. Although the fluid volumes experiencing normal stress were smaller than those experiencing shear stress, for all threshold stress values (10 Pa, 50 Pa and 100 Pa), normal stress volumes were in existance and were not negligible. When thresholds for RBC and vWf deformation were considered, the fluid volumes experiencing significant deformation were larger for normal stress as compared with shear stress. Exposure times to the shear stress deformation regions were larger than exposures to the normal stress deformations; nevertheless, the normal stress exposure times were between 0.87 and 2.5 ms which are sufficient to cause cell and protein deformation. In conclusion, the fluid within rotary VADs experiences more shear stress at much higher magnitudes as compared with normal stress. However, there is a significant volume of normal stress, with a magnitude and exposure time large enough to cause RBC and vWf deformation, which means that the normal stresses present are likely to be an important contributor to blood damage in

rotary VADs. Further experimental studies into the effects of normal stress on the blood components are required, and these can then be used to properly incorporate the effects of normal stress into numerical blood damage models.

Acknowledgments

DPYK received funding from the University of Bath Research Studentships and KHF received funding from The Royal Society (RG140414).

References

[1] Ambrosy AP, Fonarow GC, Butler J, Chioncel O, Greene SJ, Vaduganathan M, et al. The global health and economic burden of hospitalizations for heart failure: Lessons learned from hospitalized heart failure registries. Journal of the American College of Cardiology. 2014;63(12):1123–1133. Available from: http://dx.doi.org/10.1016/j.jacc.2013.11.053.

[2] Kirklin JK, Pagani FD, Kormos RL, Stevenson LW, Blume ED, Myers SL, et al. Eighth annual INTERMACS report: Special focus on framing the impact of adverse events. Journal of Heart and Lung Transplantation. 2017;36(10):1080–1086.

[3] Howell NJ, Lim HS. Ventricular assist device: Destination UK. BMJ Publishing Group Ltd and British Cardiovascular Society. 2015;101(14):1083–1084.

[4] Westaby S, Deng M. Continuous flow blood pumps: the new gold standard for advanced heart failure? European Journal of Cardio-Thoracic Surgery. 2013 jul;44(1):4–8. Available from: https://academic.oup.com/ejcts/article-lookup/doi/10.1093/ejcts/ezt248.

[5] Birks EJ, George RS, Hedger M, Bahrami T, Wilton P, Bowles CT, et al. Reversal of severe heart failure with a continuous-flow left ventricular assist device and pharmacological therapy: A prospective study. Circulation. 2011;123(4):381–390.

[6] Agarwal R, Murali S. Recovering the Broken-Hearted: The Ultimate (and Uncertain) Goal of Mechanical Circulatory Support. Journal of the American College of Cardiology. 2016;68(16):1753–1755. Available from: http://dx.doi.org/10.1016/j.jacc.2016.08.009.

[7] Birks EJ. The Promise of Recovery. JACC: Heart Failure. 2016;4(7):577–579.

[8] Kirklin JK, Naftel DC, Kormos RL, Pagani FD, Myers SL, Stevenson LW, et al. Interagency Registry for Mechanically Assisted Circulatory Support (INTERMACS) analysis of pump thrombosis in the HeartMate II left ventricular assist device. The Journal of heart and lung transplantation : the official publication of the International

Society for Heart Transplantation. 2014 jan;33(1):12–22. Available from: http://www.ncbi.nlm.nih.gov/pubmed/24418730.

[9] Kirklin JK, Naftel DC, Kormos RL, Stevenson LW, Pagani FD, Miller MA, et al. Fifth INTERMACS annual report: Risk factor analysis from more than 6,000 mechanical circulatory support patients. 2013 feb;32(2). Available from: http://www.ncbi.nlm.nih.gov/pubmed/23352390http://www.sciencedirect.com/science/article/pii/S105324981201457X?via{%}3Dihub.

[10] Fraser KH, Zhang T, Taskin ME, Griffith BP, Wu ZJ. A Quantitative Comparison of Mechanical Blood Damage Parameters in Rotary Ventricular Assist Devices: Shear Stress, Exposure Time and Hemolysis Index. Journal of Biomechanical Engineering. 2012;134(8):081002. Available from: http://biomechanical.asmedigitalcollection.asme.org/article.aspx?articleid=1476077.

[11] Thamsen B, Blümel B, Schaller J, Paschereit CO, Affeld K, Goubergrits L, et al. Numerical Analysis of Blood Damage Potential of the HeartMate II and HeartWare HVAD Rotary Blood Pumps. Artificial Organs. 2015;39(8):651–659.

[12] Fraser KH. Mechanical Stress Induced Blood Trauma. In: Heat Transfer and Fluid Flow in Biological Processes. London: Elsevier; 2015. p. 305–333. Available from: http://linkinghub.elsevier.com/retrieve/pii/B9780124080775000146.

[13] Kirklin JK, Naftel DC, Pagani FD, Kormos RL, Stevenson LW, Blume ED, et al. Seventh INTERMACS annual report: 15,000 patients and counting. Journal of Heart and Lung Transplantation. 2015 dec;34(12):1495–1504. Available from: http://www.ncbi.nlm.nih.gov/pubmed/26520247.

[14] Lee SJ, Yim YJ, Ahn KH. Extensional flow-based assessment of red blood cell deformability using hyperbolic converging microchannel. Biomedical Microdevices. 2009 oct;11(5):1021–1027. Available from: http://link.springer.com/10.1007/s10544-009-9319-3.

[15] Yaginuma T, Oliveira MSN, Lima R, Ishikawa T, Yamaguchi T. Human Red Blood Cell Behavior under Homogeneous Extensional Flow in a Hyperbolic-Shaped Mi-

crochannel. Biomicrofluidics. 2013;7(5):054110. Available from: http://dx.doi.org/10.1063/1.4820414.

[16] Zhao R, Antaki JF, Naik T, Bachman TN, Kameneva MV, Wu ZJ. Microscopic investigation of erythrocyte deformation dynamics. Biorheology. 2006;43(6):747–765. Available from: http://www.ncbi.nlm.nih.gov/entrez/query.fcgi?cmd=Retrieve{&}db=PubMed{&}dopt=Citation{&}list{_}uids=17148857.

[17] Down LA, Papavassiliou DV, O 'rear EA, O'Rear EA. Significance of Extensional Stresses to Red Blood Cell Lysis in a Shearing Flow. Annals of Biomedical Engineering. 2011 jun;39(6):1632–1642. Available from: http://link.springer.com/10.1007/s10439-011-0262-0https://link.springer.com/content/pdf/10.1007{%}2Fs10439-011-0262-0.pdf.

[18] Keshaviah PR. Hemolysis in the Accelerated Flow Region of an Abrupt Contraction. University of Minnesota.; 1974. Available from: https://books.google.co.uk/books?id=xfiWnQEACAAJ.

[19] Yen JH, Chen SF, Chern MK, Lu PC. the Effects of Extensional Stress on Red Blood Cell Hemolysis. Biomedical Engineering: Applications, Basis and Communications. 2015;27(05):1550042. Available from: http://www.worldscientific.com/doi/abs/10.4015/S1016237215500428.

[20] Sing CE, Alexander-Katz A. Elongational Flow Induces the Unfolding of von Willebrand Factor at Physiological Flow Rates. Biophysical Journal. 2010;98:35–37. Available from: https://www.ncbi.nlm.nih.gov/pmc/articles/PMC2862189/pdf/main.pdf.

[21] Springer TA. Von Willebrand factor, Jedi knight of the bloodstream. Blood. 2014 aug;124(9):1412–1425. Available from: http://www.ncbi.nlm.nih.gov/pubmed/24928861http://www.pubmedcentral.nih.gov/articlerender.fcgi?artid=PMC4148764.

[22] Fu H, Jiang Y, Yang D, Scheiflinger F, Wong WP, Springer TA. Flow-induced elongation of von Willebrand factor precedes tension-dependent activation [Jour-

nal Article]. Nature Communications. 2017;8(1):324. Available from: https://doi.org/10.1038/s41467-017-00230-2.

[23] Bludszuweit C. Three-Dimensional Numerical Prediction of Stress Loading of Blood Particles in a Centrifugal Pump. Artificial Organs. 1995 jul;19(7):590–596. Available from: http://doi.wiley.com/10.1111/j.1525-1594.1995.tb02386.x.

[24] Arora D, Behr M, Pasquali M. A tensor-based measure for estimating blood damage. Artificial Organs. 2004;28(11):1002–1015.

[25] Arora D, Behr M, Pasquali M. Hemolysis estimation in a centrifugal blood pump using a tensor-based measure. Artificial Organs. 2006;30(7):539–547.

[26] Pauli L, Nam J, Pasquali M, Behr M. Transient stress-based and strain-based hemolysis estimation in a simplified blood pump. International Journal for Numerical Methods in Biomedical Engineering. 2013 oct;29(10):1148–1160. Available from: http://doi.wiley.com/10.1002/cnm.2576.

[27] Wieselthaler GM, O'Driscoll G, Jansz P, Khaghani A, Strueber M. Initial clinical experience with a novel left ventricular assist device with a magnetically levitated rotor in a multi-institutional trial. The Journal of Heart and Lung Transplantation. 2010 nov;29(11):1218–1225. Available from: https://www.sciencedirect.com/science/article/pii/S1053249810003116.

[28] Thamsen B, Plamondon M, Granegger M, Schmid Daners M, Kaufmann R, Neels A, et al. Investigation of the Axial Gap Clearance in a Hydrodynamic-Passive Magnetically Levitated Rotary Blood Pump Using X-Ray Radiography. Artificial Organs. 2018;00(3):0–5. Available from: http://doi.wiley.com/10.1111/aor.13074.

[29] Shekar K, Gregory SD, Fraser JF. Mechanical circulatory support in the new era: An overview. Critical Care. 2016;20(1). Available from: http://dx.doi.org/10.1186/s13054-016-1235-3.

[30] Griffith BP, Kormos RL, Borovetz HS, Litwak K, Antaki JF, Poirier VL, et al. HeartMate II left ventricular assist system: from concept to first clinical use. The Annals of Thoracic Surgery. 2001;71(3):S116–S120.

[31] Noor MR, Ho CH, Parker KH, Simon AR, Banner NR, Bowles CT. Investigation of the Characteristics of HeartWare HVAD and Thoratec HeartMate II Under Steady and Pulsatile Flow Conditions. Artificial Organs. 2016;40(6):549–560.

[32] Malinauskas RA, Hariharan P, Day SW, Herbertson LH, Buesen M, Steinseifer U, et al. FDA Benchmark Medical Device Flow Models for CFD Validation. ASAIO Journal. 2017;63(2):150–160. Available from: http://insights.ovid.com/crossref?an=00002480-201703000-00009.

[33] Koks D. Explorations in Mathematical Physics. New York: Springer New York; 2006. p. 147–184. Available from: http://link.springer.com/10.1007/978-0-387-32793-8.

[34] Tsai H, Sussman I, Nagel R. Shear stress enhances the proteolysis of von Willebrand factor in normal plasma [Journal Article]. Blood. 1994;83(8):2171–2179. Available from: http://www.bloodjournal.org/content/bloodjournal/83/8/2171.full.pdf.

[35] Di Stasio E, De Cristofaro R. The effect of shear stress on protein conformation: Physical forces operating on biochemical systems: The case of von Willebrand factor [Journal Article]. Biophysical Chemistry. 2010;153(1):1–8. Available from: http://www.sciencedirect.com/science/article/pii/S0301462210001900.

[36] Vincentelli A, Susen S, Le Tourneau T, Six I, Fabre O, Juthier F, et al. Acquired von Willebrand Syndrome in Aortic Stenosis [Journal Article]. New England Journal of Medicine. 2003;349(4):343–349. Available from: http://www.nejm.org/doi/full/10.1056/NEJMoa022831.

[37] Zhang T, Taskin ME, Fang HB, Pampori A, Jarvik R, Griffith BP, et al. Study of Flow-Induced Hemolysis Using Novel Couette-Type Blood-Shearing Devices. Artificial Organs. 2011 dec;35(12):1180–1186. Available from: http://doi.wiley.com/10.1111/j.1525-1594.2011.01243.x.

[38] Paul R, Apel J, Klaus S, Schugner F, Schwindke P, Reul H. Shear Stress Related Blood Damage in Laminar Couette Flow. Artificial Organs. 2003 jun;27(6):517–529. Available from: http://doi.wiley.com/10.1046/j.1525-1594.2003.07103.x.

[39] Giersiepen M, Wurzinger LJ, Opitz R, Reul H. Estimation of shear stress-related blood damage in heart valve prostheses–in vitro comparison of 25 aortic valves [Journal Article]. Int J Artif Organs. 1990;13(5):300–6.

[40] Heuser G, Opitz R. A couette viscometer for short time shearing of blood. Biorheology. 1980;17(1-2):17–24. Available from: https://www.scopus.com/record/display.uri?eid=2-s2.0-0019186014{&}origin=inward{&}txGid=d58531dacc09be8ec6a143e7bada2708.

[41] Jikuya T, Tsutsui T, Shigeta O, Sankai Y, Mitsui T. Species differences in erythrocyte mechanical fragility: comparison of human, bovine, and ovine cells. ASAIO journal (American Society for Artificial Internal Organs : 1992). 1998;44(5):M452–5. Available from: http://www.ncbi.nlm.nih.gov/pubmed/9804471.

[42] Alessandra M, Zubair PHM, Kenny WQL, Haitham NY, Johann S, Katharine HF. Experimental measurement and numerical modelling of dye washout for investigation of blood residence time in ventricular assist devices [Journal Article]. The International Journal of Artificial Organs. 2018;p. 0391398817752877. Available from: https://doi.org/10.1177/0391398817752877.

[43] Taskin ME, Fraser KH, Zhang T, Wu C, Griffith BP, Wu ZJ. Evaluation of Eulerian and Lagrangian Models for Hemolysis Estimation [Journal Article]. ASAIO Journal. 2012;58(4):363–372. Available from: https://journals.lww.com/asaiojournal/Fulltext/2012/07000/Evaluation_of_Eulerian_and_Lagrangian_Models_for.11.aspx.

[44] Chiu WC, Girdhar G, Xenos M, Alemu Y, Soares JS, Einav S, et al. Thromboresistance Comparison of the HeartMate II Ventricular Assist Device With the Device Thrombogenicity Emulation-Optimized HeartAssist 5 VAD [Journal Article]. Journal of Biomechanical Engineering. 2014;136(2):021014–021014–9. Available from: http://dx.doi.org/10.1115/1.4026254.

[45] Leslie LJ, Marshall LJ, Devitt A, Hilton A, Tansley GD. Cell Exclusion in Couette Flow: Evaluation Through Flow Visualization and Mechanical Forces [Journal Article]. Artificial Organs. 2013;37(3):267–275. Available from: https://onlinelibrary.wiley.com/doi/abs/10.1111/j.1525-1594.2012.01561.x.

A Stress Tensor Coordinate Transformation

The rotation from the original velocity vector $\mathbf{u} = (u_1, u_2, u_3)$ to the velocity vector in the new coordinate system $\mathbf{u}' = (|\mathbf{u}|, 0, 0)$ is unique. The rotation matrix $\mathbf{R}$ defining the rotation from $\mathbf{u}$ to $\mathbf{u}'$ was constructed for each point in the flow field according to Rodrigues' Rotation Equation:

$$\mathbf{R} = \cos\theta\mathbf{I} + \sin\theta\mathbf{n}_\times + (1 - \cos\theta)\,\mathbf{n}\mathbf{n}^T \tag{6}$$

where θ is the angle between $\mathbf{u}$ and $\mathbf{u}'$, $\mathbf{I}$ is the identity matrix, $\mathbf{n}$ is the unit vector along the axis of rotation, and $\mathbf{n}_\times$ is the cross product matrix for $\mathbf{n}$. The cross product matrix $\mathbf{n}_\times$ and $\mathbf{n}\mathbf{n}^T$ are given by:

$$\mathbf{n}_\times = \begin{pmatrix} 0 & -n_3 & n_2 \\ n_3 & 0 & -n_1 \\ -n_2 & n_1 & 0 \end{pmatrix} \tag{7}$$

$$\mathbf{n}\mathbf{n}^T = \begin{pmatrix} n_1n_1 & n_1n_2 & n_1n_3 \\ n_2n_1 & n_2n_2 & n_2n_3 \\ n_3n_1 & n_3n_2 & n_3n_3 \end{pmatrix} \tag{8}$$

$\mathbf{n}$, $\sin\theta$ and $\cos\theta$ were found from $\mathbf{u}$ and $\mathbf{u}'$:

$$\mathbf{n} = \frac{\mathbf{u} \times \mathbf{u}'}{|\mathbf{u} \times \mathbf{u}'|} = 0\mathbf{i} + \frac{u_3}{(u_2^2 + u_3^2)^{\frac{1}{2}}}\mathbf{j} - \frac{u_2}{(u_2^2 + u_3^2)^{\frac{1}{2}}}\mathbf{k} \tag{9}$$

$$\sin\theta = \frac{|\mathbf{u} \times \mathbf{u}'|}{|\mathbf{u}|\,|\mathbf{u}'|} = \frac{\left(u_2^2 + u_3^2\right)^{\frac{1}{2}}}{|\mathbf{u}|} \tag{10}$$

$$\cos\theta = \frac{u_1}{|\mathbf{u}|} \tag{11}$$

Using Rodrigues' Rotation Equation the following rotation matrix $\mathbf{R}$ was obtained:

$$\mathbf{R} = \begin{pmatrix} \frac{u_1}{|\mathbf{u}|} & \frac{u_2}{|\mathbf{u}|} & \frac{u_3}{|\mathbf{u}|} \\ -\frac{u_2}{|\mathbf{u}|} & \frac{u_1}{|\mathbf{u}|} + \left(1 - \frac{u_1}{|\mathbf{u}|}\right)\frac{u_3^2}{u_2^2+u_3^2} & -\left(1 - \frac{u_1}{|\mathbf{u}|}\right)\frac{u_2u_3}{u_2^2+u_3^2} \\ -\frac{u_3}{|\mathbf{u}|} & -\left(1 - \frac{u_1}{|\mathbf{u}|}\right)\frac{u_3u_2}{u_2^2+u_3^2} & \frac{u_1}{|\mathbf{u}|} + \left(1 - \frac{u_1}{|\mathbf{u}|}\right)\frac{u_2^2}{u_2^2+u_3^2} \end{pmatrix} \tag{12}$$

$\mathbf{R}$ was then used to transform the strain rate tensor $\mathbf{s}_{ij}$ for all locations in the fluid domain into the local coordinate system $\mathbf{s'}_{ij}$:

$$\mathbf{s}' = \mathbf{R}\mathbf{s}\mathbf{R}^T \tag{13}$$

B Tables

Table 1: Mean exposure times of blood to the stress levels required to deform RBCs and vWf.

Blood component	VAD	stress	time /ms
RBCs	HVAD	normal (1.8 Pa)	0.87
		shear (13.4 Pa)	12
	HMII	normal (1.8 Pa)	2.1
		shear (13.4 Pa)	12
vWf	HVAD	normal (0.7 Pa)	1.1
		shear (35 Pa)	8.6
	HMII	normal (0.7 Pa)	2.5
		shear (35 Pa)	8.2

C Figure Captions

Figure 1: Geometry of the VAD flow domains: a. HVAD, example of a centrifugal flow VAD; b. HeartMate II, example of an axial flow VAD.

Figure 2: a. Data from Lee *et al* [14] shows RBC deformation occurring with both shear and elongational flow. By defining a DI that would compute evident deformation at 0.5, the threshold values were extrapolated to obtain threshold values for cell deformation at shear flow 13.4 Pa and elongational flow 1.8 Pa; b. Data from Sing *et al* [20] shows vWf deformation occurring with both shear and elongational flow. Maximum extensional percentage was defined at 27%, the threshold values were extrapolated to obtain threshold values at shear flow 10^4 s^{-1} (35 Pa) and elongational flow 200 s^{-1} (0.7 Pa).

Figure 3: Mesh sensitivity study for centrifugal VAD with coarse, medium and fine meshes respectively: a. Comparison of velocity fields; b. Comparison of volumes of shear stress at 50 Pa and 100 Pa; c. Comparison of volumes of threshold stresses for RBC deformation.

Figure 4: Comparison of calculated pressure head with the experimental results of from

Noor *et al* [31].

Figure 5: Comparison of calculated velocity in the FDA blood pump with experimental data from Malinauskas *et al* [32] for validation of the CFD method: a. 2D contour plot of experimental PIV measurements compared with velocity contour lines from our calculations (operating condition: 6 L/min and 3500 rpm); b. The velocity profile along the pump radius compared with experimental data

Figure 6: a. Shear and normal stress volumes in HVAD (centrifugal VAD) for blood damage threshold stress values; b. Regions of HVAD (centrifugal VAD) with threshold above 10 Pa and 100 Pa; c. Shear and normal stress volumes in HMII (axial VAD) for blood damage threshold stress values; d. Regions of HMII (axial VAD) with threshold above 10 Pa and 100 Pa.

Figure 7: a. Mean RBC deformation volumes and b. vWf deformation volumes over time, with error bars showing standard deviation.

Figure 8: Variation in mean RBC deformation volume with a. impeller speed, b. flow rate and c. axial gap clearance. Error bars show standard deviation in mean.

D Figures and Graphs

Figure 1

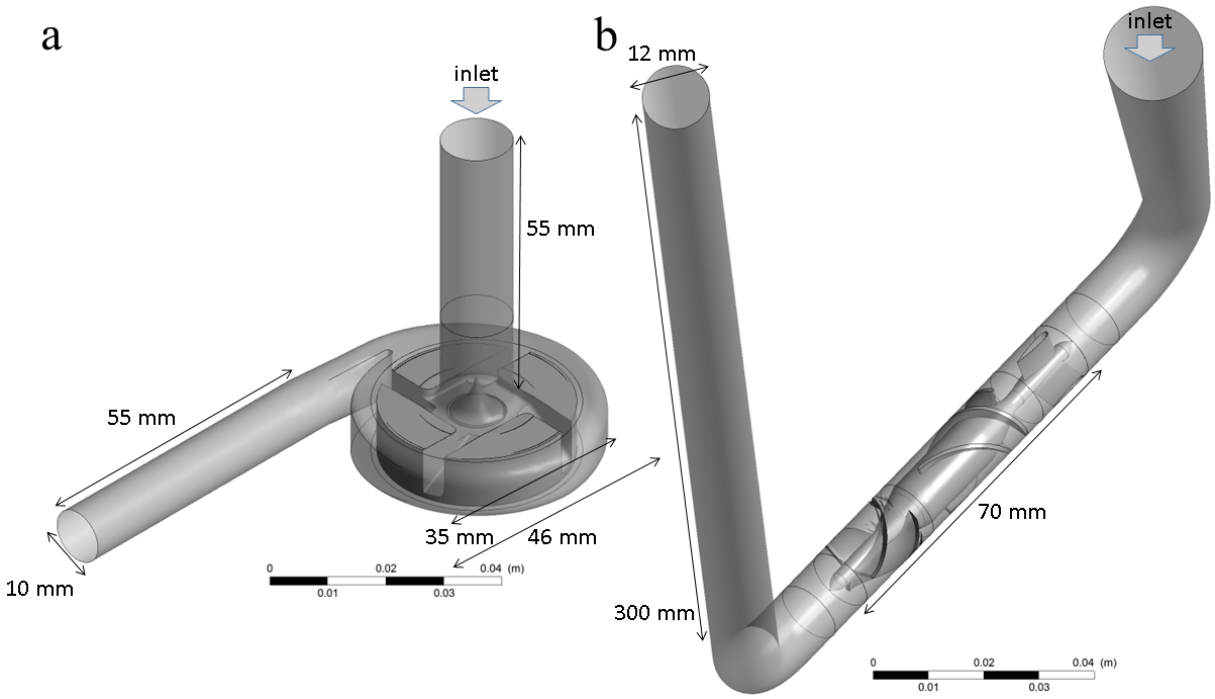

Figure 2

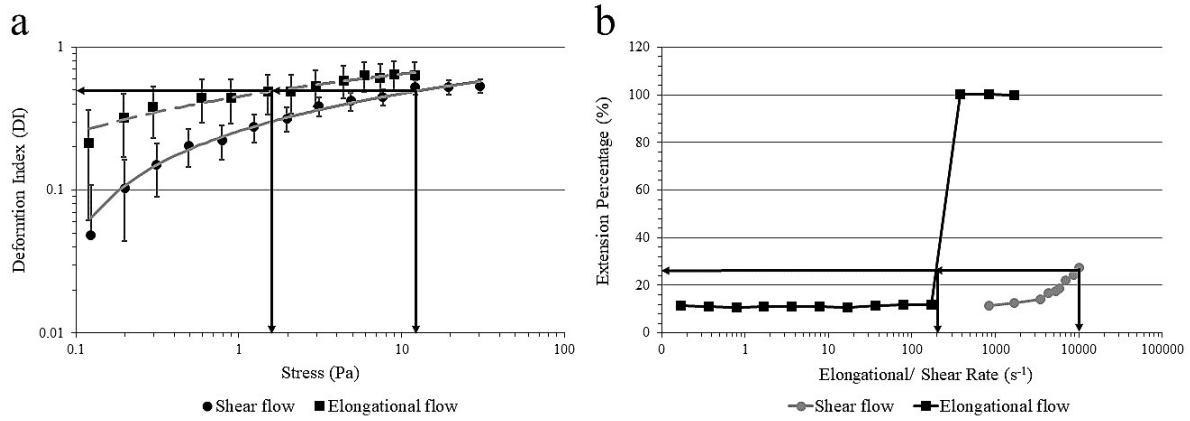

Figure 3

Figure 4

a

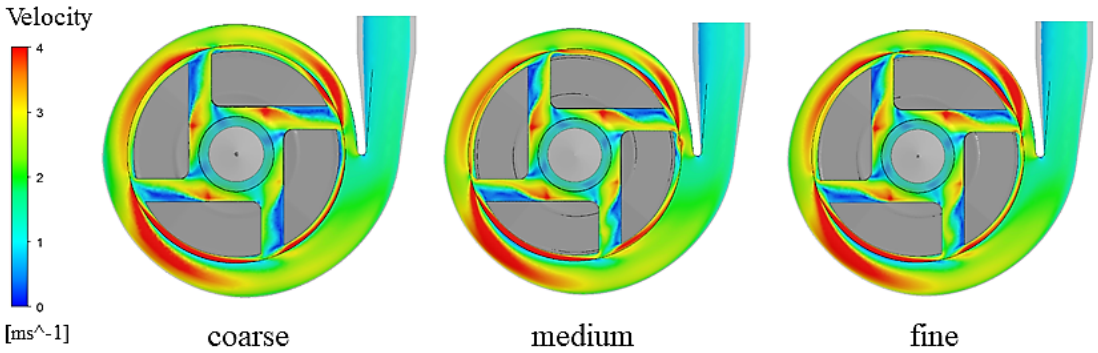
Velocity
4
3
2
1
0
[ms^-1]
coarse
medium
fine

b

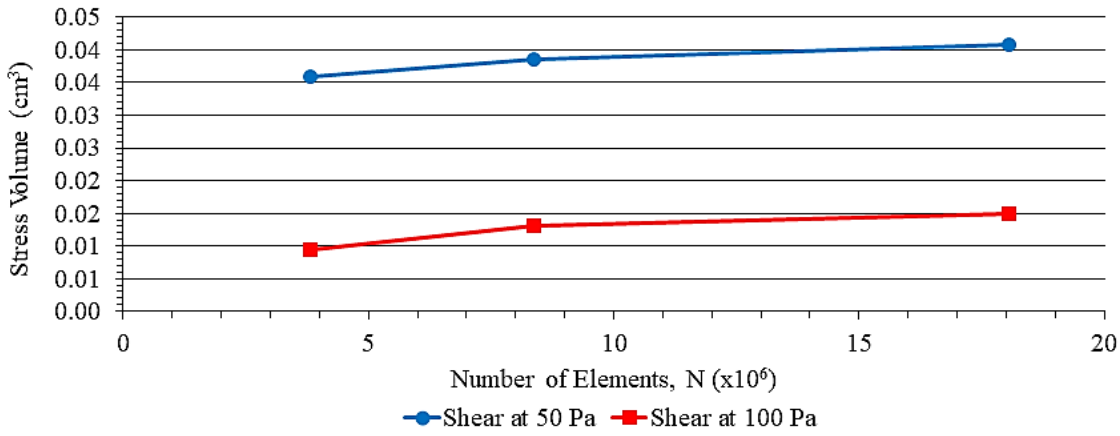
Stress Volume (cm³)
0.05
0.04
0.04
0.03
0.03
0.02
0.02
0.01
0.01
0.00
0
5
10
15
20
Number of Elements, N (x10⁶)
Shear at 50 Pa
Shear at 100 Pa

c

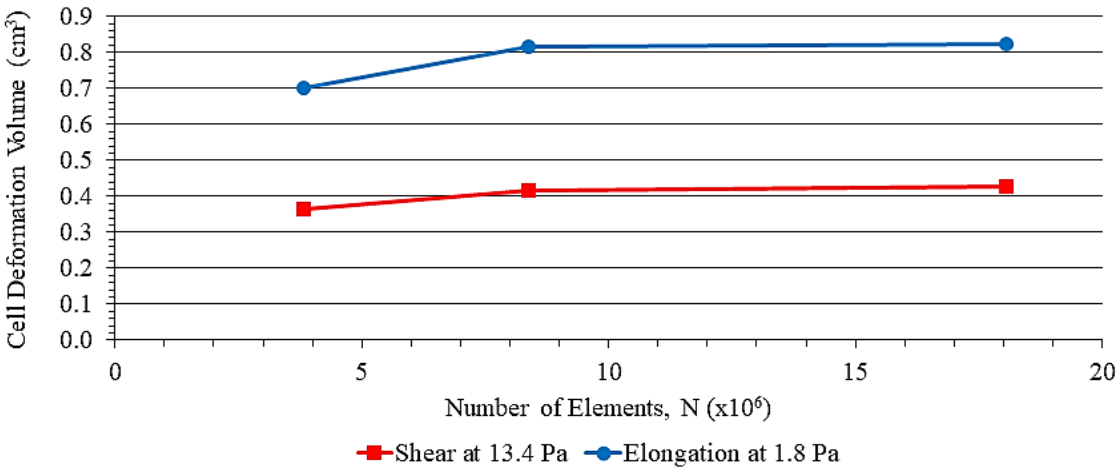
Cell Deformation Volume (cm³)
0.9
0.8
0.7
0.6
0.5
0.4
0.3
0.2
0.1
0.0
0
5
10
15
20
Number of Elements, N (x10⁶)
Shear at 13.4 Pa
Elongation at 1.8 Pa

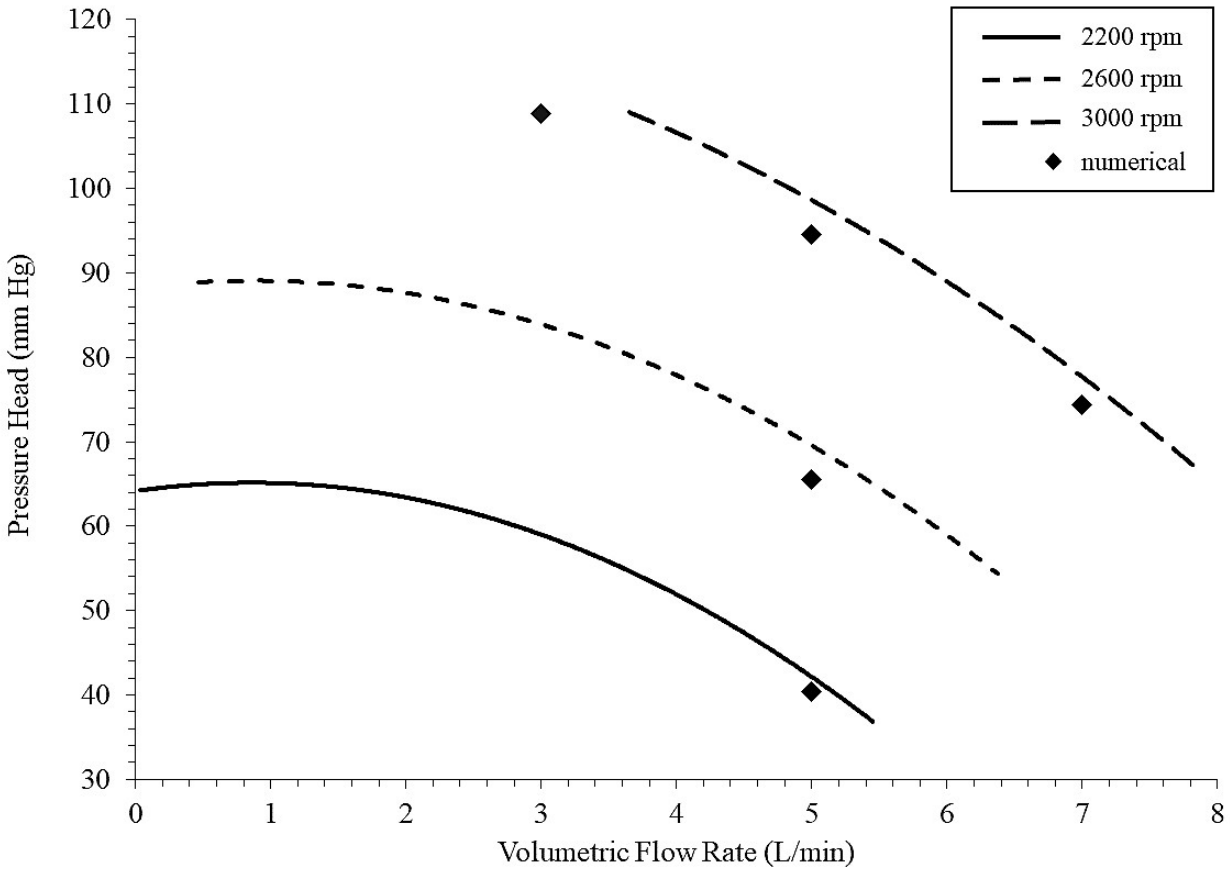
120
110
100
90
80
70
60
50
40
30
Pressure Head (mm Hg)
0
1
2
3
4
5
6
7
8
Volumetric Flow Rate (L/min)
2200 rpm
2600 rpm
3000 rpm
numerical

Figure 5

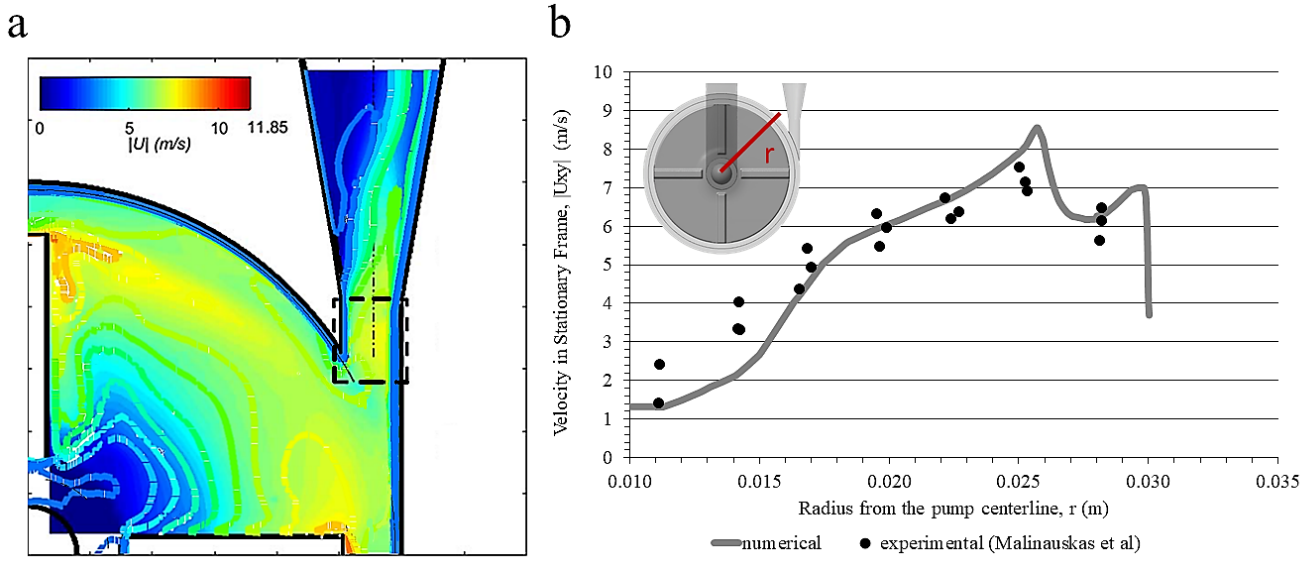

Figure 6

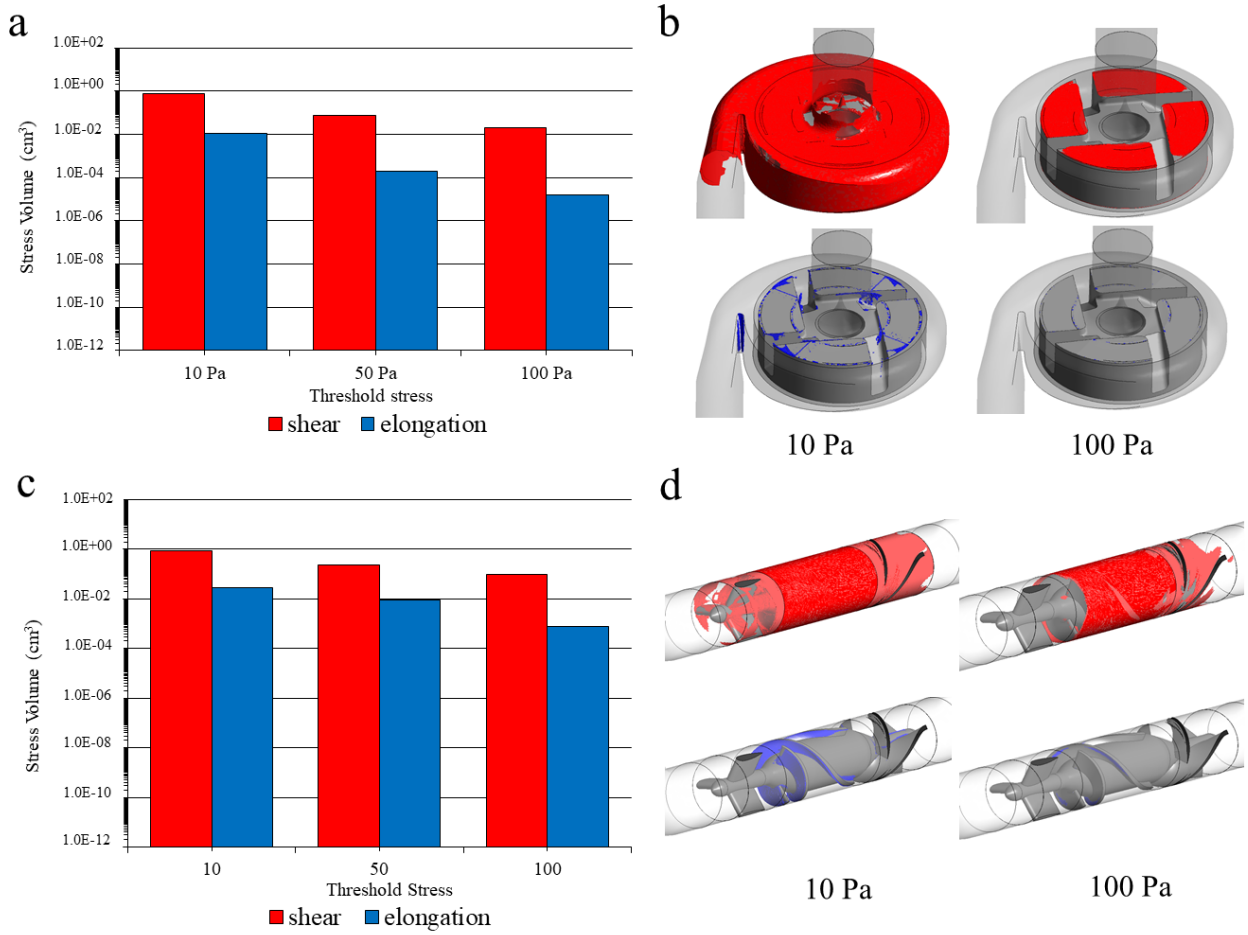

Figure 7

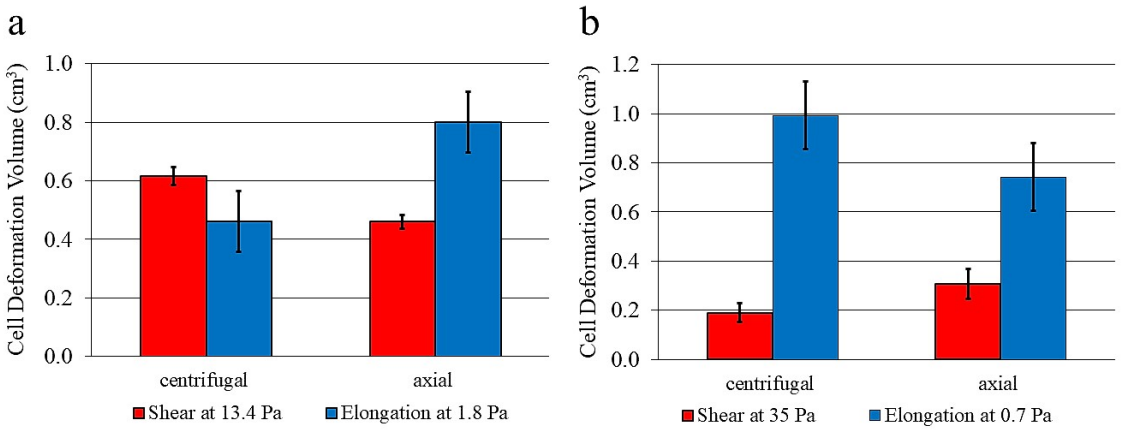

Figure 8